Nanoscale

Accepted Manuscript

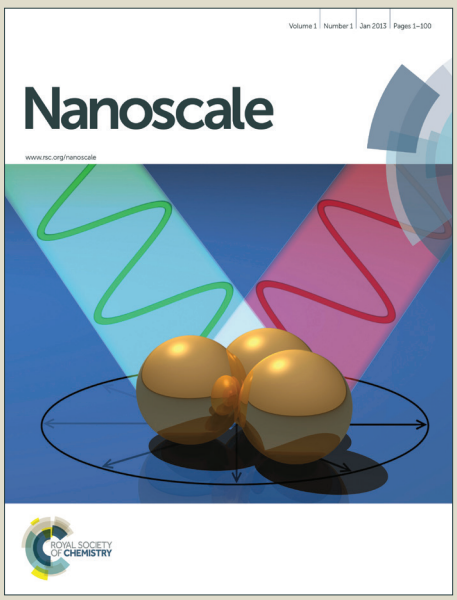

ROYAL SOCIETY OF CHEMISTRY

www.rsc.org/nanoscale

MAGNETIC GOLD NANOTRIANGLES BY MICROWAVE POLYOL SYNTHESIS

Siming Yu[1], Jordan Hachtel[2,3], Matthew Chisholm[3], Sokrates Pantelides[2,3], Anna Laromaine[1]*, Anna Roig[1]*

[1]Institut de Ciència de Materials de Barcelona, ICMAB-CSIC, Campus UAB, Bellaterra, Catalunya, E-08193 Spain
[2]Department of Physics and Astronomy, Vanderbilt University, Nashville, TN 37235 USA
[3]Materials Science and Technology Division, Oak Ridge National Laboratory, Oak Ridge, TN 37831 USA

ABSTRACT: Simple approaches to synthesize hybrid nanoparticles with magnetic and plasmonic functionalities with high control of their shape and avoiding cytotoxic reactants to target biomedical applications remain a huge challenge. Here, we report a facile, fast and bio-friendly microwave-assisted polyol route for the synthesis of a complex multi-material consisting in monodisperse gold nanotriangles around 280 nm in size uniformly decorated by superparamagnetic iron oxide nanoparticles of 5 nm. These nanotriangles are readily dispersible in water, display a strong magnetic response (10 wt% magnetic fraction) and exhibit a localized surface plasmon resonance band in the NIR region (800nm). Moreover, these hybrid particles can be easily self-assembled at the liquid-air interfaces.

KEYWORDS: magneto-plasmonic hybrid nanoparticles, nanocomposites, gold nanotriangles, iron oxide nanoparticles, microwaves synthesis.

*Corresponding authors: Anna Roig, e-mail: roig@icmab.es; Anna Laromaine, e-mail: alaromaine@icmab.es; www.icmab.es/nn; Tel.: + 34 935801853; Fax: +34 935805729.

INTRODUCTION

Large number of new health-related applications in bio-sensing, imaging and therapeutics are expected from biocompatible hybrid systems combining gold and iron oxide in a single nanoparticle displaying both magnetic and plasmonic properties[1-4]. Our work aims at the formation of heterostructures comprising superparamagnetic iron oxide nanoparticles (SPIONs) with gold nanotriangles (Au NTs), which has not been addressed so far.

The selection of SPIONs as the magnetic component is supported by their biocompatibility as well as their proved use in several nanomedicine applications such as magnetic resonance imaging[5], drug delivery[6], cell labeling[7], bio-separation[8] and hyperthermia[9]. From the other side, the optical properties and the localized surface plasmon resonance (LSPR) of gold nanoparticles (Au NP) have already motivated their biomedical uses in imaging[10], sensing[11], drug and gene delivery[12] as well as in photothermal therapies[13]. It is well established that the shape[14], size[15] and composition[16] of Au NP are crucial in determining the LSPR spectral position. The possibility to control and shift the absorption band from the ultraviolet-visible (UV-Vis) to the near-infrared region (NIR) using anisotropic Au NP is interesting since particles absorbing in the NIR heat more efficiently than spherical nanoparticles absorbing in the UV-Vis[17]. Additionally, anisotropic Au NP are highly efficient as surface-enhanced Raman spectroscopy[18]. Thus, the synthesis of Au NP with anisotropic shapes (nanorods, platonic nanoparticles, nanotriangles or nanoplates) has focused intense research efforts. In particular, gold nanotrianges are excellent nanoheaters in photothermal therapy[19,20] and effective nanomaterials for biosensing[18].

Most synthetic methods for Au NTs are based on a multi-step seed-mediated approach. Even though, important advances have been recently reported by the group of Liz-Marzan[18] on monodisperse gold nanotriangles with over 95% shape-yield after purification. This synthetic approach involves the use of the highly toxic cationic surfactant cetyltrimethylammonium bromide (CTAB)[21,22] resulting in a poorly biocompatible or very time-consuming process due to the unavoidable ligand exchange step. The polyol process based on metal reduction at high temperature by ethylene glycol in the presence of polyvinylpyrrolidone (PVP) is the other most

used approach to generate noble metal nanoparticles (particularly Ag) with controllable shapes including cubes and nanotriangles as reported by the Y. Xia's group[23-25].

Au-SPIONs nanostructures[26-31] have been obtained by one-pot[29,32] or seed mediated synthesis resulting in dumbbells[31,33], core-shell[26], nanoflowers[34], star-shape[28] or clusters[35]. Still, another strategy involves the separate fabrication of Au and iron oxide nanoparticles and the subsequent assemble by a third component[27,36]. However, the above mentioned routes mainly produce spherical Au NPs displaying an LSPR spectral band in the UV-Vis region. Regarding systems with LSPR spectral band in the NIR, Truby et al. have reported a ligand mediated self-assembly of carboxyl functionalized Au nanorods conjugated to SPIONs with a well-defined LSPR band at 900 nm[27]. Unfortunately, the method also uses CTAB or cetyltrimethylammonium chloride (CTAC) surfactants and entails poor control of the SPIONs mass fraction. Quaresma et al. described the direct formation of gold seeds on magnetite nanoparticles followed by a seed growth to form a star-shaped gold outer layer resulting in particles of poorly defined shape and a broad peak in the NIR plasmonic signal[28].

To date, attempts to exploit MW irradiation in multimaterial hybrid nanoparticles have exclusively led to sparse examples of bi-component core–shell configurations as mentioned in a recent review on microwave-assisted synthesis of colloidal inorganic nanocrystals[37]. Here, we are providing with a pioneering example of microwave heating as a non-conventional energy source for chemical synthesis of a complex multi-material. We present a rapid, facile and green (non-toxic) microwave polyol route to synthesize monodisperse Au NT-SPIONs with a triangle shape-yield of 60% prior to any purification. The Au NTs-SPIONs nanoparticles display an excellent magnetic response, arising from the high crystallinity and monodisperse size distribution SPIONs and the much required characteristic LSPR band in the NIR region. Moreover, these hybrid particles can be self-assembled as a monolayer at the liquid-air interface. Importantly, the overall time of this synthesis route is less than 40 min, no cytotoxic shape-template agents are used and the Au NT-SPIONs are readily dispersible in water. First, SPIONs were synthesized by microwave assisted thermal decomposition in the presence of

PVP. Then, the PVP-SPIONs were dispersed in an ethylene glycol solution containing $HAuCl_4$ and PVP in a microwave oven to obtain Au triangular nanocrystals decorated with a monolayer of SPIONs. Effects of PVP and the reaction conditions on the shape-yield of hybrid nanoparticles were investigated and their magnetic and plasmonic properties are reported.

EXPERIMENTAL SECTION

Materials. Iron (III) acetylacetonate ($Fe(acac)_3 \geq 97.0\%$), polyvinylpyrrolidone (PVP, average molecular weight: 10000 g/mol), hydrogen tetrachloroaurate trihydrate ($HAuCl_4 \cdot 3H_2O \geq 99.9\%$) were purchased from Sigma-Aldrich. Ethylene glycol (EG ≥ 99%) and acetone were bought from Panreac. All materials were used as received without further purification. Milli-Q water (MQ H_2O) was used in all experiments. All glassware was cleaned with aqua regia and rinsed several times with MQ H_2O.

Synthesis of PVP coated SPIONs. SPIONs with a PVP surface coating (PVP-SPIONs) were synthesized using a modified MW synthesis protocol developed in our group[38,39]. Briefly, 680 mg PVP were dissolved thoroughly in 4 mL anhydrous benzyl alcohol by continuous sonication. Then, 12.36 mg $Fe(acac)_3$ (0.035 mmol) were mixed with the above prepared solution in special MW-tubes, vortexed and sonicated for few minutes to a homogenous solution with a dark red color. Reaction tubes were then transferred to the microwave reactor and heated for 5 min at 60 ^oC and 10 min at 180 ^oC. PVP-SPIONs (5 nm in diameter) were collected by adding 30 mL acetone, centrifuged at 6000 rpm for 30 min and finally, redispersed in 4 mL EG being readily to be used for further experiments. Using the same proportions and steps but changing the MW ramp to 5 min at 60ºC and 10min at 210 ºC, we obtained PVP-SPIONs larger nanoparticles (7nm in diameter).

Synthesis of hybrid Au-SPIONs nanoparticles. Various amounts of PVP (25 mg, 50 mg, 100 mg and 150 mg) were added to the as obtained PVP-SPIONs dispersions in EG (4 mL) and sonicated to obtain homogenous mixtures. Then, 40 µL 100 mM $HAuCl_4$ was added to the mixture. The molar ratio of free PVP to $HAuCl_4$ were 0.625:1, 1.25:1, 2.5:1 and 3.75:1,

corresponding to 25 mg, 50 mg, 100 mg and 150 mg PVP respectively. The effect of MW temperature (T= 80, 100 and 120 ^{o}C) and time (t = 5, 10, 20 and 40 min) on the resulting hybrid structures were also investigated. In this synthesis, PVP is used as the capping agent (of both the SPIONS and the gold), to shape and stabilize the Au nanoparticles and as a mild reducing agent whilst EG is acting as solvent and reducing agent. As-obtained hybrid Au-SPIONs nanoparticles were washed twice with acetone to remove free PVP, collected by centrifugation at 6000 rpm for 2 min and redispersed in 2 mL MQ H_2O for further characterization. To ensure reproducibility of the results each synthetic condition was repeated three times. Table S1, in the supplementary information, summarizes the reaction conditions used and the characteristics of the obtained materials reporting the mean values of the independent experiments performed.

Materials characterization. Hydrodynamic diameter and zeta potential of PVP-SPIONs and Au-SPIONs were determined with a Zetasizer Nano ZS (Malvern) with a He/Ne 633 nm laser at 25 ^{o}C. For each sample, 3 independent measurements were performed with 15 scans for each measurement. Attenuated total reflectance Fourier transformed infrared spectra (ATR-FTIR) was performed on a Spectrum RX1 FTIR Spectrometer (Perkin Elmer, USA) in the frequency range 4000-400 cm^{-1} with a resolution of 4 cm^{-1}. Samples were isolated from the solution by centrifugation, dried in the oven and placed on the crystal surface of the ATR-FTIR equipment. Size distribution, morphology and diffraction patterns of PVP-SPIONs and Au-SPIONs were collected in a JEOL JEM-1210 electron microscope at an operating voltage of 120 KV. High-resolution transmission electron microscopy (HRTEM) was performed on a JEOL 2010F HRTEM along with scanning transmission electron microscopy (STEM) performed on a Nion UltraSTEM operating a 200 kV. TEM samples were prepared by placing several drops of the samples on the copper grid, blotting the copper grid with a filter paper and let the water to completely evaporate at room temperature. Typically, at least 300 different nanoparticles were counted with ImageJ to depict the size histogram distribution and the mean particle size. Scanning electron microscopy (SEM) analysis of Au-SPIONs hybrid nanostructures were performed on a QUANTA FEI 200 FEG-ESEM. A self-assembled gold monolayer was

obtained using a hexane:ethanol (2:3) and water mixture, similarly as it has been previously described[18]. The assembled Au NTs-SPIONs monolayer was then transferred to a TEM grid for further characterization. Ultraviolet-visible-near infrared (UV-Vis-NIR) spectra were collected on a Cary-5000 UV-Vis-NIR spectrophotometer. To determine the iron concentration, samples were sonicated for 10 min in an ultrasound bath. An aliquot of the sample was diluted with HCl (1%) and the iron content of the resulting solution was determined by flame absorption spectroscopy (air-acetylene) with a Perkin-Elmer 2100 spectrometer in a triplicate essay. Superconductive Quantum Interference Device (SQUID) measurements were recorded on a magnetometer (Quantum Design MPMS5XL) to determine the magnetization of the PVP-SPIONs and the Au-SPIONs. Typically, 150 μL of an aqueous solution with known Fe concentration was placed and dried in the polycarbonate capsule to be inserted in the SQUID magnetometer sample holder. Magnetization curves, of the PVP-SPIONs and the hybrid Au-SPIONs, were recorded at 5K as a function of applied magnetic field up to 6 Tesla. Zero-field-cooling and field cooling magnetization values (ZFC-FC) as a function of temperature in a magnetic field of 50 Oe were also recorded.

RESULTS AND DISCUSSION

The experimental procedure for the synthesis of hybrid gold nanotriangles (Au NTs) decorated with superparamagnetic iron oxide nanoparticles (SPIONs) using microwave heating involved two main steps: i) preparation of PVP coated SPIONs in benzyl alcohol and ii) the growth of gold crystals in ethylene glycol in the presence of the PVP-SPIONs.

Microwave-assisted synthesis of PVP-SPIONs

Fast synthesis of SPIONs by microwave-assisted thermal decomposition with narrow particle size distribution and high saturation magnetization values were previously reported in our group[38,39]. Here, we have adapted such protocol for the *in situ* fabrication of SPIONs coated with PVP (PVP-SPIONs). Briefly, PVP was dissolved thoroughly in anhydrous benzyl alcohol. Then, the $Fe(acac)_3$ was added to the solution and heated for 5 min at 60 ^{o}C and 10 min at 180

^{o}C in the microwave reactor. PVP-SPIONs were precipitated in acetone, centrifuged and re-dispersed in ethylene glycol being ready for further use. Figure S1a shows a TEM image of the as-obtained PVP-SPIONs. The inset of Figure S1a contains a selected area electron diffraction (SAED) pattern indexed to an inverse spinel structure of maghemite. The mean particle size was determined at 5 ± 1 nm (Figure S1b). PVP-SPIONs are dispersible and stable in water and their hydrodynamic diameter, provided by dynamic light scattering (DLS), is about 14 nm as shown in Figure S1c. Magnetometry, M(H) hysteresis loops at 5K, shows a saturation magnetization value at 74 emu/g_{Fe2O3} (Figure S1d) and a remanent magnetization of 21 emu/g_{Fe2O3} (inset in Figure S1d). Larger PVP-SPIONs (7.3 ± 1.6 nm) can be obtained by increasing the synthesis temperature to 210 ^{o}C. Their corresponding characterization is provided in the Supplementary Information (Figure S2). PVP coating on SPIONs surface was confirmed by FTIR (Figure S3).

Microwave-assisted synthesis of hybrid Au NTs-SPIONs nanoparticles

A homogenized mixture of PVP-SPIONs, $HAuCl_4 \cdot 3H_2O$ and PVP (PVP:$HAuCl_4$ molar ratio=0.625:1) in ethylene glycol was placed in the microwave reactor at 120 ºC for 10 min. After MW synthesis, the black color of the PVP-SPIONs dispersion in EG (Figure 1a) changed to orange (Figure 1b) pointing to the successful synthesis of Au nanoparticles. The analysis of several SEM images showed that a remarkable 60% yield of gold nanotriangles decorated with SPIONs can be obtained prior to any purification (Figure S4). Thus, this synthetic approach offers a facile and fast route to synthesize hybrid magneto-plasmonic nanotriangles. Moreover, when considering hexagons as a planar form of truncated triangles, the resulting yield is over 75%. The remaining nanoparticles are a mixture of platonic structures (icosahedrons and cubes) (28%) and smaller rounded nanoparticles (2%) (Figure S4). Using an external magnet we can easily and completely separate, in less than 10 min, the dispersed product (Figure 1c) indicating that the Au nanoparticles are physically connected to the SPIONs with PVP as the chemical binder. High resolution TEM and STEM images are included as Figures 1d and 1e confirming that the structure is composed of a single Au NT core with well-defined equilateral shape with its surface uniformly decorated by a monolayer of SPIONs. Figure 1e further reveals the

homogeneity of the SPIONs coating on the Au NT surface. The inset of Figure 1e contains the Fast-Fourier-Transform (FFT) of the STEM image. The visible circular rings pattern in the FFT indicates that the SPIONS are randomly oriented with respect to the Au-NT and that there is no epitaxial relationship.

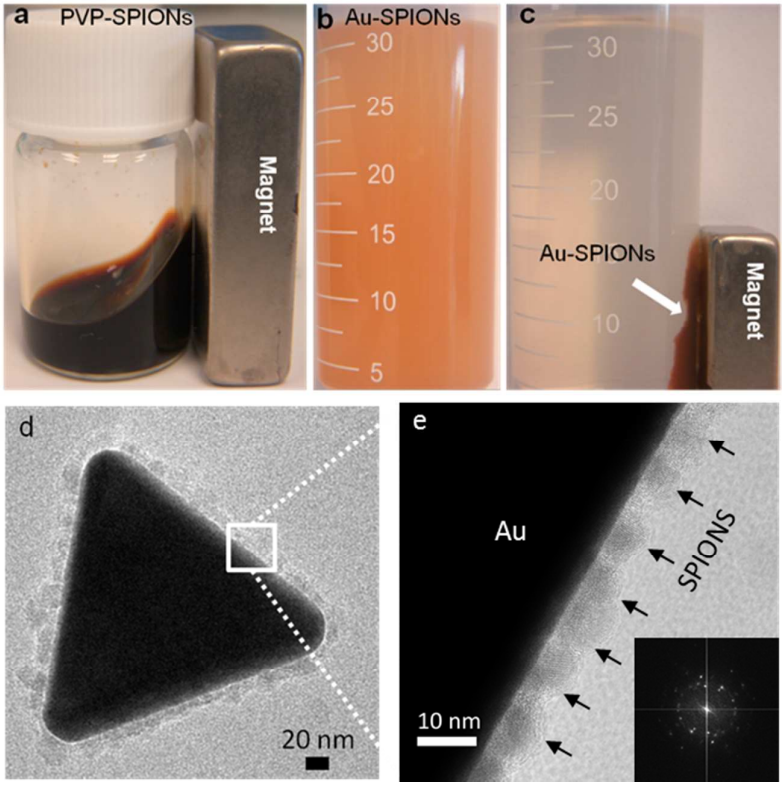

Figure 1. Digital images a) PVP-SPIONs aqueous solution shows a dark brown color and a strong magnetic response. b) Au NTs-SPIONs nanocomposites dispersed in water display an orange color. c) Au NTs-SPIONs nanocomposites collected by an external magnet in less than 10 min. d) HR-TEM image of a single Au NT-SPIONs nanocomposite. e) High magnification STEM image of a single Au NT where a monolayer of crystalline SPIONs is clearly visualized. The inset contains the Fast Fourier Transform (FFT) of the STEM image, and shows that the SPIONs are oriented randomly and have no epitaxial relationship with the Au-NT.

Due to the presence of the PVP, the Au NTs-SPIONs can be self-assembled into a continuous gold monolayer[18] that is visible to the naked eye, as shown in Figure 2a. The closed packed triangles are depicted in Figure 2b. Triangles have a mean lateral size of 284 ± 43 nm resulting from the fitting of the size histogram to a Gaussian distribution (Figure 2c). The UV-Vis-NIR spectra in Figure 2d clearly showed a major NIR LSPR band at 800 nm, which is characteristic of anisotropic Au nanostructures (e.g. Au nanorods or nanotriangles). The LSPR band at 800

nm is however rather broad and we argue it can be related to the presence of other anisotropic Au structures or to the surface roughness endowed by the SPIONs decoration. Nevertheless the latter assumption was previously shown to have little effect on the absorption spectral band[27]. Besides the NIR LSPR band found at 800 nm, a small shoulder of LSPR band can be seen around 570 nm assigned to the small fraction of spherical Au-SPIONs NPs. It is noteworthy that in previous synthetic approaches reporting for Au NT, spherical Au NPs are a common by-product[19,40] whereas in our case, spherical Au NPs account only for 2% of the final product.

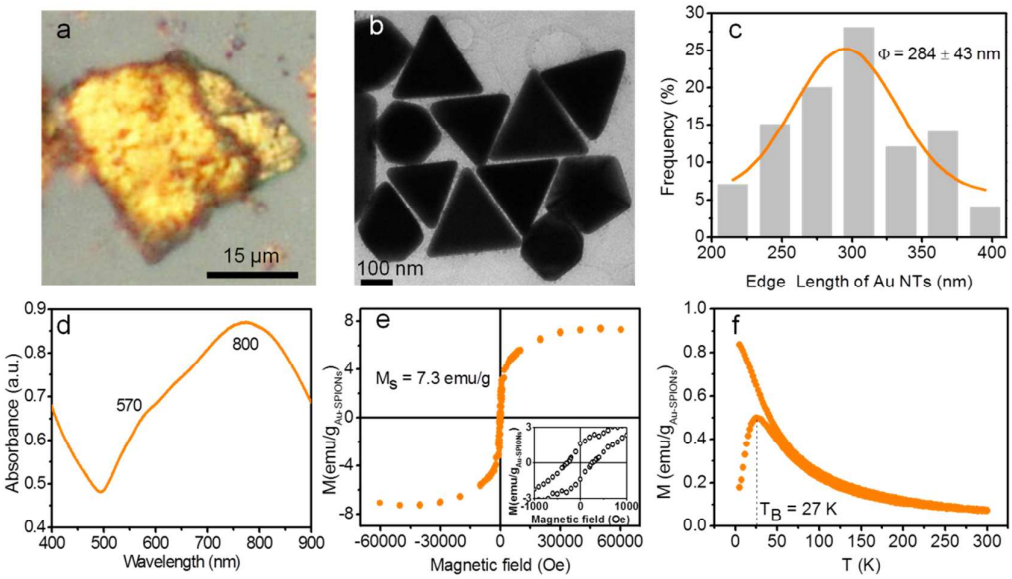

Figure 2. a) Optical microscope image of the monolayer assembled at the liquid-air interface. b) TEM image of the assembled Au NTs-SPIONs. c) Size histogram of the Au NTs computed from several TEM images. d) UV-Vis-NIR spectra of the Au NTs-SPIONs nanocomposites. e) Magnetization curve of the Au NTs-SPIONs nanocomposites at 5K. f) ZFC-FC curve of the same system at 50 Oe.

SPIONs endow magnetic functionality to the hybrids constructs[33] and their magnetic properties were recorded in a superconducting quantum interference device (SQUID) magnetometer. The magnetization curve (M-H loop) and zero-field-cooling curve are depicted in Figures 2e and 2f. Compared to PVP-SPIONs a significant decrease in the saturation magnetization value was observed due to the diamagnetic nature of the gold (7.3 emu/g) (Figure 2e). From the saturation magnetization values of Au NT-SPIONs and of PVP-SPIONs (74 emu/g, see Figure S1) we can

determine that 10% mass ratio of SPIONs are decorating the gold surface. Besides, when plotting the normalized hysteresis loops of both materials, the curves are superimposing confirming that the gold is not affecting the magnetic behavior of the SPIONs (Figure S5). ZFC/FC curves of Au-SPIONs hybrid nanoparticles were also measured at an applied field of 50 Oe. Curves indicate PVP-SPIONs in the hybrid material maintain their superparamagnetic character with a blocking temperature of 27 K (Figure 2f).

Thus, we have shown that based on the heating selectivity and the increase of the molecular motion, complex nanostructured materials can be fabricated by microwaves-assisted thermal decomposition in short time. Even though, a deep mechanistic understanding of the growth mechanism is beyond the scope of this work, we interrogated how the amount of free PVP, reaction temperature and time affect the hybrid nanocrystals synthesis.

Effect of PVP

Previous reports from the Xia's group indicated the significant role of PVP in the formation of Ag anisotropic structures in EG and in water[25,41]. We have also identified the PVP:$HAuCl_4$ molar ratio as a key parameter to control the yield of gold nanotriangles. The following reactions were performed at 120 ^{o}C for 10 min. MW heating of $HAuCl_4$ in EG in the absence of PVP and PVP-SPIONs resulted in large Au aggregates (Figure S6). MW heating of $HAuCl_4$ in EG with PVP but without PVP-SPIONs resulted in spherical Au NPs of 9 nm mean size (Figures S7a and S7b). Thus, free PVP and PVP-SPIONs play crucial roles in the formation of anisotropic Au-SPIONs hybrids. Later, different amounts of PVP, 25, 50, 100 and 150 mg corresponding to PVP/$HAuCl_4$ molar ratios equal to 0.625:1, 1.25:1 2.5:1 3.5:1, were used. The yield of Au NTs-SPIONs hybrid nanoparticles significantly increases by gradually decreasing the amount of PVP in the reaction, reaching a maximum of 60% when 25 mg PVP was added (Figure 3a). Additionally, the number of Au spheres and hexagons decrease while the percentage of platonic structures was almost not affected (Figure 3a). TEM images of the nanocomposites obtained at different PVP amounts (Figure 3c-1 to 3c-5) and the shape

histogram compiled from several TEM images confirmed these observations (Figure 3a). If we compile the histogram considering planar structures (triangles and hexagons), platonic structures and spheres, it indicates that planar shapes increase at the expense of spheres at lower PVP molar ratios. Differently, when the amount of PVP is further increased to 150 mg, only individual and small round shape Au and SPIONs are observed (Figure 3c-5). HR-TEM images reveal that Au NPs and SPIONs bound to each other form pairs or trimers (Figure S7c). When no extra free PVP was added and the PVP supply was solely from the one attached to the SPIONs surface, the hybrids formed were also spherical with a testimonial presence of some hexagons and with the LSPR band maximum at 573 nm (Figure 3a-1 and Figure S8). This observation indicates the need of free PVP as structuring agent for the nanotriangles to nucleate and further grow. Moreover, independent of the shape of the Au NPs, a monolayer of SPIONs was always visible on the Au surface (Figure S9).

UV-Vis-NIR spectra of the Au-SPIONs hybrids obtained using different PVP amounts are displayed in Figure 3b. LSPR peak red shifted when decreasing the amount of PVP, with a maximum LSPR peak at 800 nm observed when 25 mg PVP was used. Indeed, larger size of Au NTs for the lowest amount of PVP was confirmed by TEM. In particular, the edge length of the Au NTs obtained with 100 mg of PVP was 150 nm while increased to 280 nm when 25 mg of PVP were used (Figure S10a). Hydrodynamic diameter (D_h) of Au NP-SPIONs nanocrystals confirmed those findings (Figure S10b). Therefore, we ascribe the red shift of the NIR LSPR peak to the increase edge length and the improved purity of the Au NT. Figure 3b also displays a narrow absorption peak in the UV-Vis region (535 nm) from the small spherical Au-SPIONs obtained using 150 mg of PVP. Additionally PVP-SPIONs play a protective role to the gold nanoparticles since the absorption spectra recorded for the as-obtained materials and for materials kept during 3 months were identical indicating that no major reshaping of the Au particles occurs (Figure S10c).

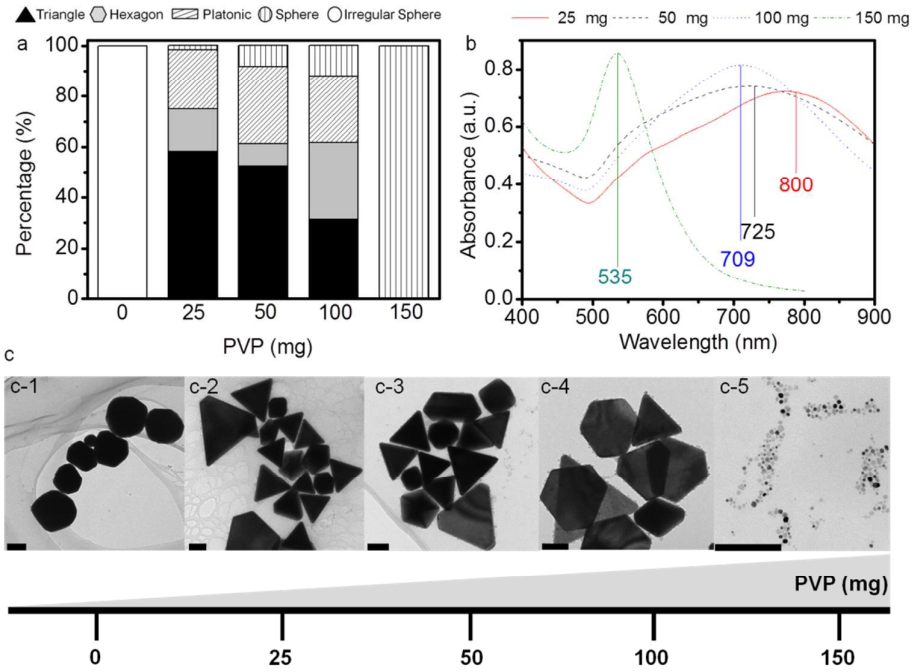

Figure 3. a) Shape-yields of Au-SPIONs nanocomposites at a free PVP amount of 0 mg, 25mg, 50mg, 100 mg and 150 mg. b) UV-Vis-NIR spectra of Au-SPIONs nanocomposites at a free PVP amount of 25mg, 50mg, 100 mg and 150 mg. c) Representative TEM images of Au-SPIONs nanocomposites (scale bar represents 100 nm), c-1to c-5 correspond to free PVP amount of 25mg, 50mg, 100 mg and 150 mg, respectively.

Effect of temperature and reaction time

Effect of the temperature on the shape-yield was investigated by using 100 mg PVP, 10 min reaction time and synthetic temperatures of 80, 100 and 120 ^{o}C, results are shown in Figure 4. Notice that those are rather low temperatures in comparison to the 160 ^{o}C used in the polyol synthesis of Ag nanotriangles. Upon increasing the temperature, the most significant observation was the gradual decrease in the percentage of Au spheres and the gradual increase in the number of Au planar structures. The percentage of the Au NTs-SPIONs hybrid is around 32% for the three temperatures. LSPR peak of the Au-SPIONs nanocomposites displayed a gradual red shift while increasing temperature (Figure 4b). Main LSPR peak centered at around 649 nm for hybrids at 80 ^{o}C, while shifted to 709 nm when temperature increased to 120 ^{o}C. The observed red shift is likely related to the increased number of anisotropic Au nanostructures since Au spheres accounted for nearly 25% of the total at 80 ^{o}C and only 12% at 120 ^{o}C. Moreover, DLS measurements showed that the hydrodynamic size (D_h) gradually increases with

the increasing temperature (Figure S11). A mean size of 122 nm was observed at 80 °C that increased to 169 nm when the synthesis was performed at 120 °C.

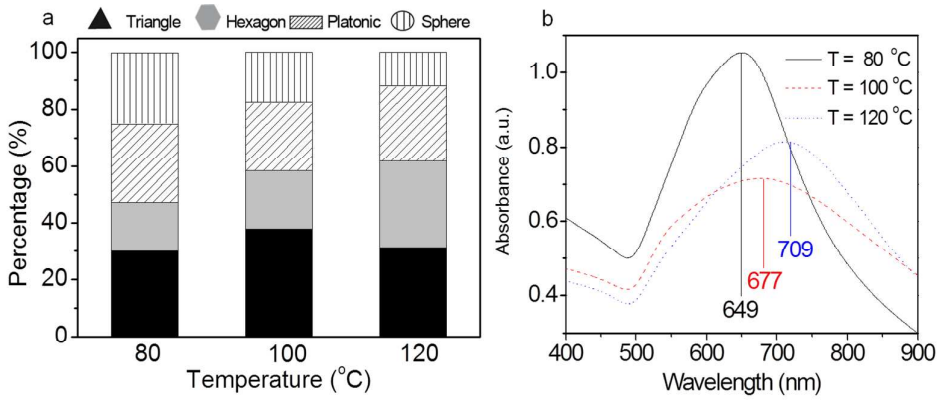

Figure 4. a) Shape-yields of Au-SPIONs nanocomposites obtained at different temperatures. b) UV-Vis-NIR spectra of those materials.

Reaction time on the shape-yield of different Au-SPIONs nanostructures seems to have little influence aside for a slight decrease of the number of spheres as the reaction time is extended. (Figure S12a). LSPR band shows a blue shift when reaction extended (Figure S12b), which is in contrast to the results obtained from the other synthetic methods as the reaction evolves[24]. However, our observation agrees with the results reported by de la Fuente's group[19] that assigns this slight blue shift to the evolution from the well-defined triangles to the tip-truncated ones. Indeed, formation of truncated Au triangles can be inferred from the small decrease of D_h size of Au-SPIONs hybrid nanostructures obtained at longer reaction time (Figure S12c).

Figure 5 schematizes a simplified mechanism proposed for the formation of triangular shape Au nanoparticles although at this point we can not provide an explanation of the break of the initial symmetry to avoid spherical growth. Notice that, microwave heating of $HAuCl_4$ in EG in the presence of PVP leads to the reduction of Au (III) to Au (0), where both EG and PVP served as reducing reagents[32]. When Au (0) nucleates, free PVP adsorbs to all golds surfaces, due to the strong affinity of Au surface to the nitrogen of the PVP, resulting in small spherical Au NPs. However, when introducing PVP-SPIONs to the same system, Au anisotropic nanostructures with their surfaces decorated with SPIONs were produced. It is known that the shape of the

initial nuclei is of great importance in determining the structure of the final products[41]. PVP-SPIONs are negatively charged ($Z_{potential}$ = - 30 mV) exposing the OH^- group of the PVP. The polar OH rich zone on the SPIONs surface can served as preferential sites to nucleate the gold in a similar manner as we have previously reported for the *in-situ* synthesis of nanoparticles on hydroxyl rich substrates[42,43]. As a result, Au seeds with a triangular shape are likely to occur. Those initially formed triangular Au seeds serve as the nucleation site for the later reduced Au atoms to grow on. During crystal grow, free PVP will preferentially adsorb to the facets with the lowest energy. Selectively adsorbing on the {111} facets (top and bottom facets of Au nanocrystals) while {100} facets (three side facets) continued growing at a faster rate. Finally, depending on the ratio of {111} to {100} facets on the side faces, either triangular or tip-truncated Au nanostructures can be obtained[41]. Moreover, decreasing the amount of PVP could lead to the slower generation of Au nuclei, which in turn resulted in the larger edge length of the anisotropic Au nanostructures like triangles. The elongated edge length of the Au NTs can be evidenced from the larger D_h size determined by DLS measurements (Figure S10b) and the red shift of LSPR peak observed in the NIR region (Figure 3b). Besides, we also observed that increasing the PVP amount higher than 100 mg resulted in the formation of Au-SPIONs pairs instead of anisotropic Au-SPIONs hybrid nanostructures. Thus, excess of PVP suppresses the formation of the initial triangular SPIONs-Au clusters and leads to the formation of small individual Au NPs partially attached to SPIONs. At the PVP concentrations, temperatures and synthesis times scanned here we have observed that a constant fraction (around 25%) of hybrid nanoparticles self-nucleate into nucleus of different forms, octahedron or icosahedrons. These shapes are thermodynamically favorable as reported for the silver structures[41].

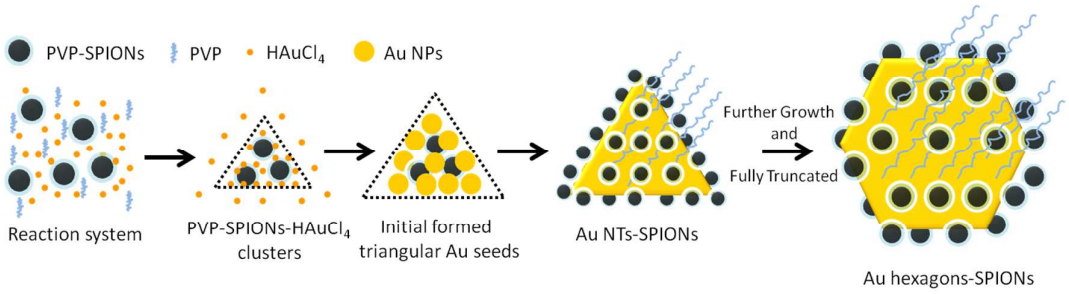

Figure 5. Schematic illustration of the formation of anisotropic Au-SPIONs hybrid nanomaterials. A proposed mechanism for the formation of Au NTs-SPIONs, truncated Au NTs-SPIONs and Au hexagons-SPIONs.

CONCLUSIONS

Here, we are providing with a pioneering example of microwave heating as a non-conventional energy source for the chemical synthesis of a complex multi-material. We have presented a facile, fast and bio-friendly polyol method to obtain Au-SPIONs hybrid nanoparticles readily dispersible in water. Remarkably and prior to any purification, 60% shape-yield of Au triangles with their surfaces homogenously decorated with a monolayer of SPIONs was achieved. We hypothesized that hydroxyls on the PVP-SPIONs form preferential hot spots that served as selective nucleation sites determining the shape of the initial Au seeds. The Au NTs-SPIONs nanoparticles display an excellent magnetic response, arising from the high crystallinity and monodisperse size distribution of SPIONs and the much required characteristic LSPR band in the NIR region. Moreover, these hybrid particles readily self-assemble as a monolayer in liquid-air interfaces. In addition, our process allows a certain degree of control of the anisotropic Au-SPIONs nanocomposites with tunable optical properties by judicious choice of the synthesis parameters such as the PVP amount, reaction temperature and reaction time.

Acknowledgements

This research was partially funded by Spanish Ministry of Economy (MAT2012-35324), the Generalitat de Catalunya (2014SGR213) and the People Program of the European Commission (grant agreement nº 303630, co-funded by the European Social Fund). Authors also acknowledge support of the Ramon y Cajal grant RYC-2010-06082 (AL), the Chinese Scholarship Council fellowship (SMY, 201206150053) and the COST Action MP1202, NSF-EPS-1004083 (JH, STP), NSF-TN-SCORE (JH, STP). Work at Oak Ridge supported by the

Department of Energy, Office of Science, Basic Energy Sciences, Materials Sciences and Engineering Division.

References

(1) Lee, J.; Yang, J.; Ko, H.; Oh, S.; Kang, J.; Son, J.; Lee, K.; Lee, S. W.; Yoon, H. G.; Suh, J. S.; Huh, Y. M.; Haam, S. *Advanced Functional Materials* **2008**, *18*, 258.

(2) Xu, C.; Wang, B.; Sun, S. *Journal of the American Chemical Society* **2009**, *131*, 4216.

(3) Wang, C.; Irudayaraj, J. *Small* **2010**, *6*, 283.

(4) Mohammad, F.; Balaji, G.; Weber, A.; Uppu, R. M.; Kumar, C. S. S. R. *The Journal of Physical Chemistry C* **2010**, *114*, 19194.

(5) Taboada, E.; Solanas, R.; Rodríguez, E.; Weissleder, R.; Roig, A. *Advanced Functional Materials* **2009**, *19*, 2319.

(6) Guo, S.; Li, D.; Zhang, L.; Li, J.; Wang, E. *Biomaterials* **2009**, *30*, 1881.

(7) Carenza, E.; Barceló, V.; Morancho, A.; Montaner, J.; Rosell, A.; Roig, A. *Acta Biomaterialia* **2014**, *10*, 3775.

(8) Yu, C.-J.; Lin, C.-Y.; Liu, C.-H.; Cheng, T.-L.; Tseng, W.-L. *Biosensors and Bioelectronics* **2010**, *26*, 913.

(9) Di Corato, R.; Espinosa, A.; Lartigue, L.; Tharaud, M.; Chat, S.; Pellegrino, T.; Ménager, C.; Gazeau, F.; Wilhelm, C. *Biomaterials* **2014**, *35*, 6400.

(10) Luke, G.; Yeager, D.; Emelianov, S. *Ann Biomed Eng* **2012**, *40*, 422.

(11) Xu, L.; Kuang, H.; Xu, C.; Ma, W.; Wang, L.; Kotov, N. A. *Journal of the American Chemical Society* **2011**, *134*, 1699.

(12) Duncan, B.; Kim, C.; Rotello, V. M. *Journal of Controlled Release* **2010**, *148*, 122.

(13) Hirsch, L. R.; Stafford, R. J.; Bankson, J. A.; Sershen, S. R.; Rivera, B.; Price, R. E.; Hazle, J. D.; Halas, N. J.; West, J. L. *Proceedings of the National Academy of Sciences* **2003**, *100*, 13549.

(14) Bastús, N. G.; Comenge, J.; Puntes, V. c. *Langmuir* **2011**, *27*, 11098.

(15) DuChene, J. S.; Niu, W.; Abendroth, J. M.; Sun, Q.; Zhao, W.; Huo, F.; Wei, W. D. *Chemistry of Materials* **2012**, *25*, 1392.

(16) Liz-Marzán, L. M. *Langmuir* **2005**, *22*, 32.

(17) Govorov, A. O.; Richardson, H. H. *Nano Today* **2007**, *2*, 30.

(18) Scarabelli, L.; Coronado-Puchau, M.; Giner-Casares, J. J.; Langer, J.; Liz-Marzán, L. M. *ACS Nano* **2014**, *8*, 5833.

(19) Pelaz, B.; Grazu, V.; Ibarra, A.; Magen, C.; del Pino, P.; de la Fuente, J. M. *Langmuir* **2012**, *28*, 8965.

(20) Perez-Hernandez, M.; del Pino, P.; Mitchell, S. G.; Moros, M.; Stepien, G.; Pelaz, B.; Parak, W. J.; Galvez, E. M.; Pardo, J.; De La Fuente, J. M. *ACS nano* **2014**.

(21) Sau, T. K.; Murphy, C. J. *Journal of the American Chemical Society* **2004**, *126*, 8648.

(22) Millstone, J. E.; Métraux, G. S.; Mirkin, C. A. *Advanced Functional Materials* **2006**, *16*, 1209.

(23) Wiley, B.; Sun, Y.; Mayers, B.; Xia, Y. *Chemistry – A European Journal* **2005**, *11*, 454.

(24) Washio, I.; Xiong, Y.; Yin, Y.; Xia, Y. *Advanced Materials* **2006**, *18*, 1745.

(25) Sun, Y.; Xia, Y. *Science* **2002**, *298*, 2176.

(26) Shi, W.; Zeng, H.; Sahoo, Y.; Ohulchanskyy, T. Y.; Ding, Y.; Wang, Z. L.; Swihart, M.; Prasad, P. N. *Nano Letters* **2006**, *6*, 875.

(27) Truby, R. L.; Emelianov, S. Y.; Homan, K. A. *Langmuir* **2013**, *29*, 2465.

(28) Quaresma, P.; Osorio, I.; Doria, G.; Carvalho, P. A.; Pereira, A.; Langer, J.; Araujo, J. P.; Pastoriza-Santos, I.; Liz-Marzan, L. M.; Franco, R.; Baptista, P. V.; Pereira, E. *RSC Advances* **2014**, *4*, 3659.

(29) Mezni, A.; Balti, I.; Mlayah, A.; Jouini, N.; Smiri, L. S. *The Journal of Physical Chemistry C* **2013**, *117*, 16166.

(30) Brollo, M. E. F.; Lopez-Ruiz, R.; Muraca, D.; Figueroa, S. J. A.; Pirota, K. R.; Knobel, M. *Sci. Rep.* **2014**, *4*.

(31) George, C.; Dorfs, D.; Bertoni, G.; Falqui, A.; Genovese, A.; Pellegrino, T.; Roig, A.; Quarta, A.; Comparelli, R.; Curri, M. L.; Cingolani, R.; Manna, L. *Journal of the American Chemical Society* **2011**, *133*, 2205.

(32) Zhang, Y.; Ding, H.; Liu, Y.; Pan, S.; Luo, Y.; Li, G. *Journal of Materials Chemistry* **2012**, *22*, 10779.

(33) Yu, H.; Chen, M.; Rice, P. M.; Wang, S. X.; White, R. L.; Sun, S. *Nano Letters* **2005**, *5*, 379.

(34) Wei, Y.; Klajn, R.; Pinchuk, A. O.; Grzybowski, B. A. *Small* **2008**, *4*, 1635.

(35) Butoescu, N.; Jordan, O.; Burdet, P.; Stadelmann, P.; Petri-Fink, A.; Hofmann, H.; Doelker, E. *European Journal of Pharmaceutics and Biopharmaceutics* **2009**, *72*, 529.

(36) Schmidtke, C.; Kloust, H.; Bastus, N. G.; Merkl, J.-P.; Tran, H.; Flessau, S.; Feld, A.; Schotten, T.; Weller, H. *Nanoscale* **2013**, *5*, 11783.

(37) Baghbanzadeh, M.; Carbone, L.; Cozzoli, P. D.; Kappe, C. O. *Angewandte Chemie International Edition* **2011**, *50*, 11312.

(38) Pascu, O.; Carenza, E.; Gich, M.; Estradé, S.; Peiró, F.; Herranz, G.; Roig, A. *The Journal of Physical Chemistry C* **2012**, *116*, 15108.

(39) Yu, S.-M.; Laromaine, A.; Roig, A. *J Nanopart Res* **2014**, *16*, 1.

(40) Malikova, N.; Pastoriza-Santos, I.; Schierhorn, M.; Kotov, N. A.; Liz-Marzán, L. M. *Langmuir* **2002**, *18*, 3694.

(41) Xiong, Y.; Washio, I.; Chen, J.; Sadilek, M.; Xia, Y. *Angewandte Chemie International Edition* **2007**, *46*, 4917.

(42) Pascu, O.; Caicedo, J. M.; Lopez-Garcia, M.; Canalejas, V.; Blanco, A.; Lopez, C.; Arbiol, J.; Fontcuberta, J.; Roig, A.; Herranz, G. *Nanoscale* **2011**, *3*, 4811.

(43) Zeng, M.; Laromaine, A.; Feng, W.; Levkin, P. A.; Roig, A. *Journal of Materials Chemistry C* **2014**, *2*, 6312.

TOC: Facile, fast and bio-friendly microwave-assisted polyol route to synthesize high yield magnetic gold nanotriangles